Corrosion Resistance of Superalloys in the Temperature Range 800-1300 °F (430-700 °C)

F. SAEGUSA and D. A. SHORES

The corrosion behavior of several nickel- and cobalt-base superalloys was examined in accelerated oxidation tests at temperatures between 800 and 1300 °F (430 and 700 °C) in O_2 + 0.15 pct SO_2 atmospheres and in the presence of corrosive deposits. The compositions of the deposits were calculated from thermodynamic considerations to represent the combustion products of several typical types of fuels. Penetration measurements on metallographic cross sections showed that at temperatures above 1050 °F (570 °C) the rate of corrosion increased rapidly. Metallographic inspection revealed thick, porous, non-protective oxide scales with extensive cracks, but no internal sulfides or chromium depleted zones. The extent of corrosion was dependent on the composition of the deposit; those containing Na, V, and Pb appeared to be about equally aggressive to most of the alloys, while the K-bearing deposit was most aggressive and the deposit containing Ca and Mg was least aggressive.

INTRODUCTION

Superalloys are generally used in gas turbines for service at temperatures above 1400 °F (760 °C). The ever-increasing firing temperature needed for increased thermal efficiency and output has led to the development of a water-cooled gas turbine. The advantages of water-cooling are: (1) improved cycle performance by higher firing temperature and pressure levels, (2) increased reliability by reducing component metal temperature, and (3) fuel flexibility to allow the use of lower grade fuels. An issue of some concern is the possibility of hot corrosion induced by deposits from the combustion of contaminated fuels.

Although the mechanism of hot corrosion has not been entirely clarified, the phenomenon of corrosion is generally divided into two steps. The first step is the deposition of corrosive ash on the protective oxide covering the metal surface. This corrosive ash is formed during combustion with fuels containing metal contaminants and sulfur. Air for combustion may also contain contaminants. The second step is the reaction of condensate with the oxide scale, causing it to become porous and non-protective, and leading to internal oxidation or sulfidation. Accelerated rates of attack are generally observed only when the deposit is liquid or contains liquid components.

The chemical composition of corrosive deposits can be predicted from the composition of minor components in the fuel and the combustion conditions. Several different contaminant levels for typical fuels were considered in this work. The compositions of the resulting deposits on the first stage water-cooled bucket were calculated from thermodynamics aided by the use of a computer program. These calculations were verified by analysis of actual condensates from the small combustor test rig.

The work reported here was supported by the Electric Power Research Industries as part of the Water-Cooled Gas

F. SAEGUSA and D. A. SHORES are with the General Electric Company, Gas Turbine Division and Corporate Research and Development, respectively, Schenectady, NY 12345.

ISSN 0162-9719/82/0601-0016$00.75/0

Turbine Development Program. It was undertaken to determine a maximum skin temperature of candidate materials at which the corrosion rate is low enough to permit the water-cooled turbine bucket to survive for 83,000 hours, while exposed to the very high temperature combustion products from contaminated gas or liquid fuels.

CONDENSATE CHEMISTRY

Sulfur is the most common contaminant of hydrocarbon fuels and occurs in amounts ranging from about 0.5 wt. pct in distillate oils to 5.0 wt. pct in coal. During combustion, in the presence of excess oxygen, sulfur is oxidized to SO_2 and SO_3. The ratio of these gases is dependent on temperature and the availability of catalytically active surfaces. These gases can react with alkali metals, especially sodium, and alkaline-earth metals such as calcium to form very stable sulfates which are extremely corrosive when present as a liquid. In addition, other heavy metal contaminants, such as vanadium and lead, also form in deposits and may exacerbate corrosion.

Five different fuel compositions were selected for computation: (A) contaminated distillate, (B) residual oil, (C) contaminated distillate without vanadium, (D) coal-derived oil (COED), and (F) H-coal boiler grade oil. COED is a multistaged process in which coal is first pyrolyzed to produce a volatile pitch-like product which is then hydrogenated to give a range of liquid fuels. The H-coal process involves a direct catalytic hydrogenation of coal. In the boiler fuel mode of operation, heavy fuel with some ash content is produced somewhat analogous to petroleum residual fuel.

The contamination levels are given in wt. ppm and are listed in the left side of Table I. The composition of the gaseous and condensed phases produced from combustion can be calculated by a thermodynamic analysis with an aid of computer program similar to the NASA's Chemical Equilibrium Computer Program,[1] which is based on the minimization of free energy in chemical equilibrium while maintaining a proper mass balance between the reactant and products.

The program allows calculation of the chemical equilibrium composition of a homogeneous or heterogeneous system for assigned thermodynamic states, such as temperature-pressure or enthalpy-pressure. The computer results are listed in the right side of Table I as condensate composition, expressed in the mole pct for each set of contaminant levels at a temperature of 1200 °F (650 °C) and a static pressure of seven atmospheres, these being the nominal turbine conditions selected as a basis for the pot furnace tests. Although the equilibrium SO_2-to-SO_3 ratio at 1200 °F (650 °C) is far different from that expected in the high temperature combustion gas stream, it has been found that deposit compositions often reflect gas compositions corresponding to the temperature of the deposit. The calculation of deposit compositions in a steep temperature gradient is a complex problem and is beyond the scope of the present

Table I. Contaminant Levels in Fuel and Predicted Composition of Deposit

Fuel	Impurities (ppm)							Deposit Composition (mole pct)							
	S (pct)	Na	K	V	Pb	Mg	Ca	Deposit*	Na_2SO_4	K_2SO_4	$CaSO_4$	$MgSO_4$	$PbSO_4$	V_2O_5	$NaVO_3$
Contaminated Distillate	1	2		1	2			A	75.2				24.8		
Residual Oil	1	20		50	5			B	92				5.1	3.1	0.3
Contaminated Distillate Without Vanadium	1	2			2			C	75				25		
Coal-Derived Oil (COED)	0.11	4.8	1.5		0.4			D	84	15			1		
Coal-Derived, Producing Lowest Melting Deposit	NA							E	53	12		35			
H-Coal Boiler Grade	1.5	5	16		1	3	6	F	18.4	34.5	25.9	20.9	0.8		
								H	17.2	32.2	23.7	19.5	7.5		
Clean Distillate to Give Pure Sodium Sulfate	—	—	—	—	—	—	—	I	100						
								J**	83.7	14.4	0.9		0.9		

* Atmosphere was O_2 + 0.15% SO_2
** Deposit D with Ca Added

work. The experimental approach adopted represents a reasonable compromise.

There are limited thermodynamic data available for all the participating species, and some assumptions were involved in the computation. Therefore, it was necessary to verify the calculated results by a test in a pressurized simulated combustor. A small combustor test stand (mini-rig) was used which models a gas turbine combustion system and first stage nozzle up to the throat region. An additive solution, consisting of organo-metallic salts dissolved in benzene and carbon disulfide, was blended with No. 2 fuel oil to provide the required level of sulfur and other contaminants. The deposits were collected on the test specimen nozzle during combustion and were chemically analyzed afterward. Limited tests showed fairly good agreement between the observed and predicted composition.

EXPERIMENTAL PROCEDURE

A series of hot corrosion tests with salt deposits have been carried out on twelve alloys representing candidate materials for both the bucket skin and substrate. The nominal compositions of the alloys are listed in Table II. Specimens were cut in coupons of ¼ inch × ½ inch × 0.030 inch (0.64 cm × 1.27 cm × 0.076 cm) to 0.060 inch (0.15 cm) with faces parallel to within 0.0002 inch (5 μm). Prior to testing the coupons were polished through 600 grit paper. After measuring the thicknesses with a micrometer, the coupons were sprayed with an aqueous solution containing the appropriate concentration of components for the desired deposit.

Exposure Test In Simulated Deposit

The experimental apparatus is shown in a photograph in Figure 1. The furnaces were maintained at a constant temperature to within ±2 °F. Specimens were hung from a stainless steel fixture suspended in a mullite tube as shown in Figure 2. A set of coupons, comprising 8 to 10 different alloys, was exposed in a slowly flowing stream of O_2-0.15 pct SO_2 (10 to 20 ml/min) in a pot furnace at a temperature of 800, 925, 1050, 1100, 1175 or 1300 °F (430, 500, 570, 590, 640 or 700 °C). This environment approximately simulated the oxygen and sulfur potentials expected in the combustion gas at operating pressure.

In order to apply the deposits as a thin uniform layer, the components were dissolved in an aqueous solution and sprayed on the coupons with an air brush. An ethylenediamine tetra-acetic acid (EDTA) complexing agent was employed to keep Pb and Ca in solution in the presence of sulfates. Upon exposure at test temperature, the EDTA was quickly burned away and the SO_2 in the atmosphere converted the components to their respective sulfates. Chemical analysis and X-ray diffraction generally confirmed that deposits with the desired composition were obtained.

The deposits were replenished by respraying the coupons three times per week, a procedure which also served to

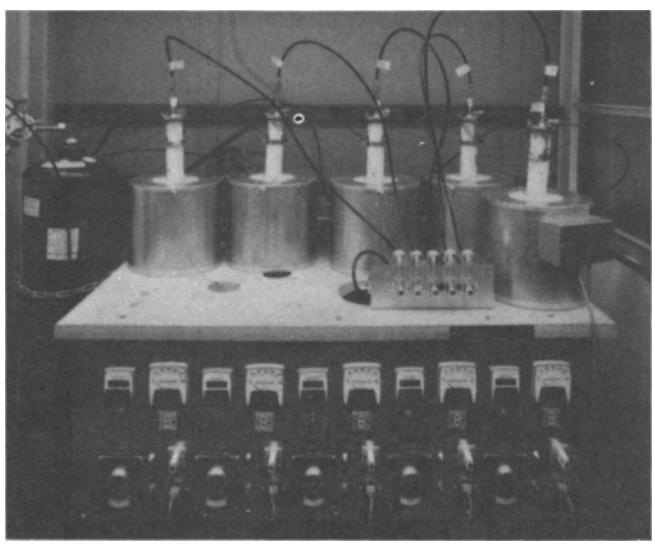

Fig. 1 — Experimental assembly of exposure furnaces.

Table II. Nominal Composition of Candidate Alloys (Wt. Pct)

Alloy	Ni	Co	Fe	Cr	Al	Ti	Mo	W	C	Mn	Other
U-500	Bal.	18.5	—	18	2.9	2.9	4	—	0.08	—	
FeCrAlY	—	—	Bal.	25	4	—	—	—	—	—	1Y
Hast-X	Bal.	1.5	18.5	22	—	—	9	0.6	0.1	0.5	0.5 Si
IN-738	Bal.	8.5	—	16	3.4	3.4	1.7	2.6	0.17	—	1.7 Ta, 0.9 Cb
IN-617	Bal.	12.5	—	22	1	—	9	—	0.07	—	
IN-718	Bal.	—	18.5	18.6	0.4	0.9	3.1	—	0.04	0.2	0.3 Si, 5.0 Cb
HS-188	22	Bal.	1.5	22	—	—	—	14	0.1	0.75	0.4 Si, 0.08 La
A-286	26	—	Bal.	15	0.2	2	1.3	—	0.05	1.35	0.5 Si
GTD-111	Bal.	9.5	—	0.14	3	5	1.5	4	0.17	—	3.0 Ta
IN-671	Bal.	—	—	50	—	0.3	—	—	—	—	
Hast-S	Bal.	—	1.0	15.5	0.2	—	14.5	—	0.03	0.50	0.4 Si
IN-825	41	—	Bal.	21.5	0.1	0.9	3.0	—	0.03	0.50	2.25 Cu

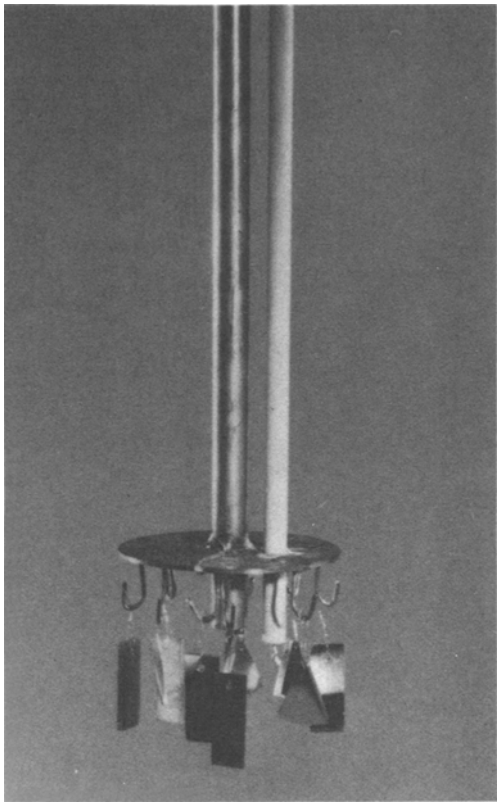

Fig. 2—Specimen holder with gas inlet tube in the center.

thermally cycle the samples. After given exposure times, the coupons were sectioned and examined metallographically, and the thickness of remaining metal was measured with a stage micrometer. The reported penetrations are an average of at least three measurements per coupon.

EXPERIMENTAL RESULTS

The results of these tests are given in Table III in terms of mils penetration/side at 1000 hours. Some of the data were taken after approximately 500 hours exposure and were

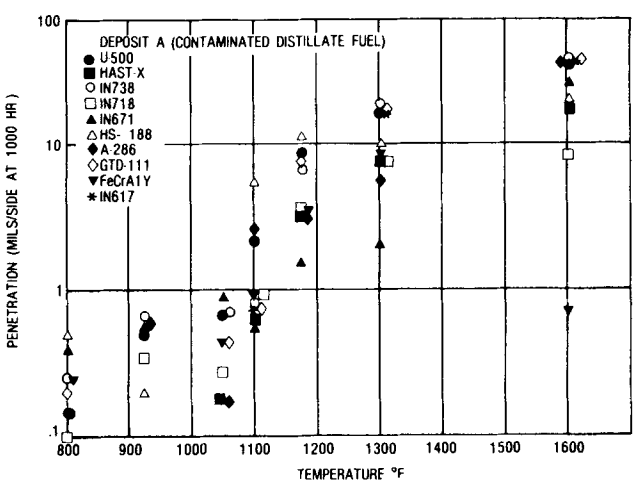

Fig. 3—Penetration with deposit A at 800 to 1600 °F.

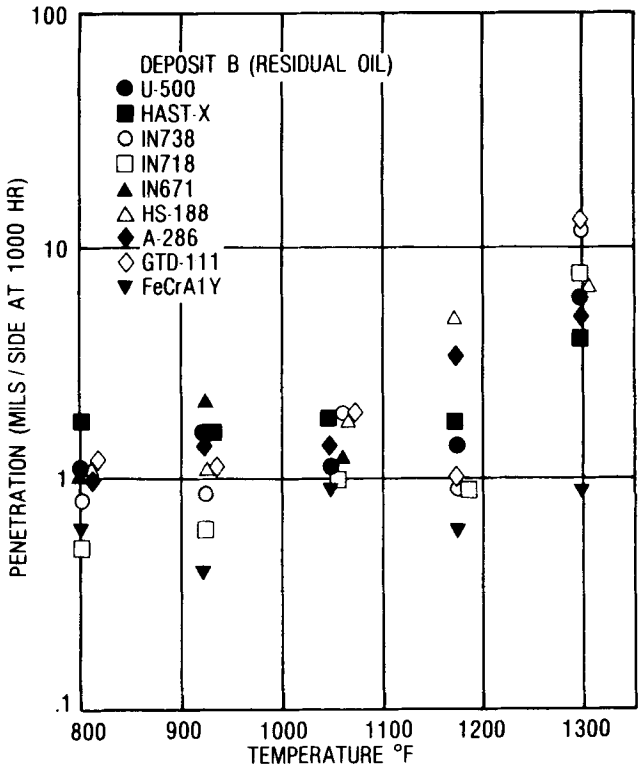

Fig. 4—Penetration with deposit B at 800 to 1300 °F.

extrapolated linearly to 1000 hours. The penetration data in each deposit are plotted against temperature. Deposits A, B, C, D, E, and H are shown in Figures 3, 4, 5, 6, 7, and 8, respectively. It may be readily seen that the corrosion data

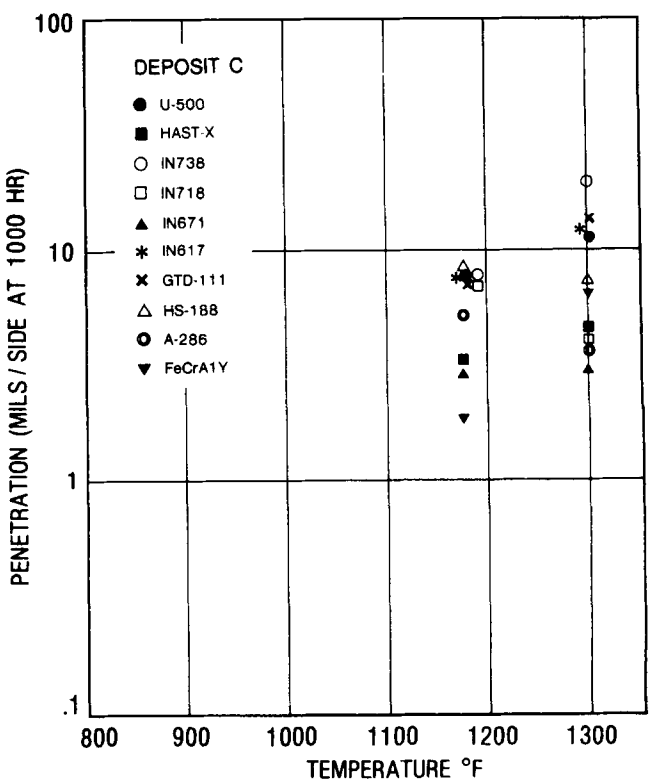

Fig. 5—Penetration with deposit C at 1175 to 1300 °F.

Table III. Observed Penetrations. (Mils per Side at 1000 Hours)

Alloy	Deposit A						
	800 °F	925 °F	1050 °F	1100 °F	1175 °F	1300 °F	1600 °F
U-500	−0.3	0.5	0.68	2.2	8.3	16.4	35.1
FeCrAlY	0.25	0.07	0.45	0.84	3.4	8.4	0.72
Hast X	−0.1	−0.3	0.18	0.65	3.2	7.6	17.3
IN-738	0.25	0.67	0.7	0.84	1.6	19.4	38.6
IN-617	—	—	—	0.74	—	—	36.5
IN-718	0.1	0.35	0.27	0.93	3.6	7.8	8.1
HS-188	0.5	0.2	0.0	5.5	11.6	16.0	19.9
A-286	0.15	0.6	0.18	2.6	3.2	5.6	37.2
GTD-111	0.2	−0.08	0.45	0.74	7.8	16.8	38.1
IN-671	0.4	0.35	0.91	0.56	1.5	2.0	26.5

Alloy	Deposit B					Deposit C	
	800 °F	925 °F	1050 °F	1175 °F	1300 °F	1175 °F	1300 °F
U-500	1.1	1.6	1.1	1.4	6.6	7.8	11.4
FeCrAlY	0.6	0.4	0.9	0.6	0.9	1.9	6.6
Hast X	1.8	1.6	1.8	1.7	3.9	3.4	4.6
IN-738	0.8	0.9	1.9	0.9	11.8	7.6	11.0
IN-617	—	—	—	—	—	7.7	12.1
IN-718	0.5	0.6	1.0	0.9	7.8	7.3	4.1
HS-188	1.1	1.1	1.8	5.0	6.6	8.7	7.6
A-286	1.0	1.4	1.4	4.4	5.0	5.2	3.8
GTD-111	1.2	1.6	1.9	1.0	13.0	7.6	14.0
IN-671	1.0	2.2	1.2	0	0	3.0	3.1

Alloy	Deposit D					Deposit I	Deposit J
	925 °F	1050 °F	1110 °F	1175 °F	1300 °F	1300 °F	1300 °F
U-500	0.68	—	15.7	20.9	41.5	—	5.4
FeCrAlY	0.31	3.04	8.0	8.41	8.03	—	—
Hast X	0.89	2.1	11.1	40.7	26.6	—	—
IN-738	0.78	1.5	18.5	17.9	25.2	11.2	9.2
IN-617	0.68	—	19.2	24.7	26.8	—	5.1
IN-718	1.30	1.85	11.3	7.65	21.8	—	2.5
HS-188	0.48	—	13.8	14.1	18.4	—	—
A-286	0.62	6.25	17.2	16.2	31.5	15.4	—
GTD-111	0.89	1.5	37.9	13.8	31.1	10.9	7.6
IN-671	0.48	0.55	1.44	1.76	0.80	1.7	0.70
Hast-S	1.5	1.5	—	—	—	—	—

Alloy	Deposit E				Deposit H			
	925 °F	1050 °F	1175 °F	1300 °F	925 °F	1050 °F	1175 °F	1300 °F
U-500	1.7	1.9	6.5	8.4	—	2.2	2.1	1.8
IN-738	1.8	1.3	3.6	5.2	0.66	0.70	1.7	1.7
IN-617	2.7	2.1	5.4	6.4	1.0	5.5	1.9	2.8
IN-718	1.6	2.1	3.2	4.8	1.2	2.1	2.0	1.8
HS-188	1.1	2.2	5.9	16.7	0.68	5.6	1.7	2.4
A-286	1.0	1.8	6.2	9.1	1.1	1.8	4.0	4.7
GTD-111	1.0	2.7	4.6	7.9	1.0	0.40	2.0	2.6
IN-671	1.0	1.9	1.5	1.6	1.3	0.69	1.1	3.1
Hast-S	1.9	2.5	3.8	6.3	1.7	6.2	1.6	4.2
IN-825	1.5	1.6	7.2	8.7	1.8	1.0	1.5	3.2

can be largely divided into two temperature regions: 1100 °F (590 °C) and above, where substantial attack occurred, and 1050 °F (570 °C) and below, where essentially no measurable attack was observed. Figure 9 shows field observations in the temperature range of 1000 to 1300 °F (540 to 700 °C), and despite appreciable scatter, there is general agreement between the laboratory and field data. The typical appearance of a sample after a substantial attack at tem-

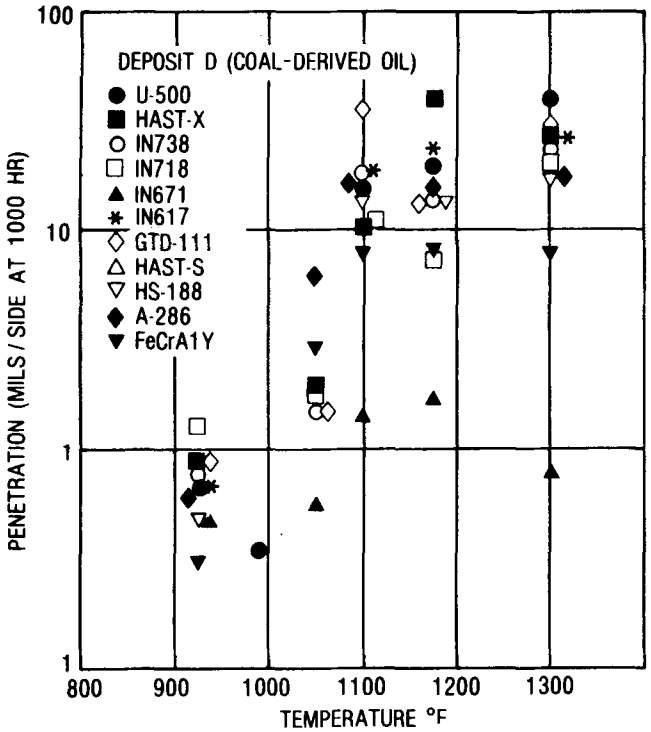

Fig. 6—Penetration with deposit D at 925 to 1300 °F.

peratures above 1100 °F (590 °C) showed a thick, porous, and unprotective oxide scale that had cracked extensively, with some pieces having spalled off.

General observations at the two highest temperatures (1300 °F (700 °C) and 1175 °F (640 °C)) show that the deposits A, B, C, and E appear to be about equally aggressive to most of the alloys, deposit D is significantly more corrosive, and H is least corrosive. The rate of attack with deposit J is appreciably less than that with D and on a par with that from E, which contains no Pb. Figure 10 compares the penetration values at 1300 °F (700 °C) for four alloys (U-

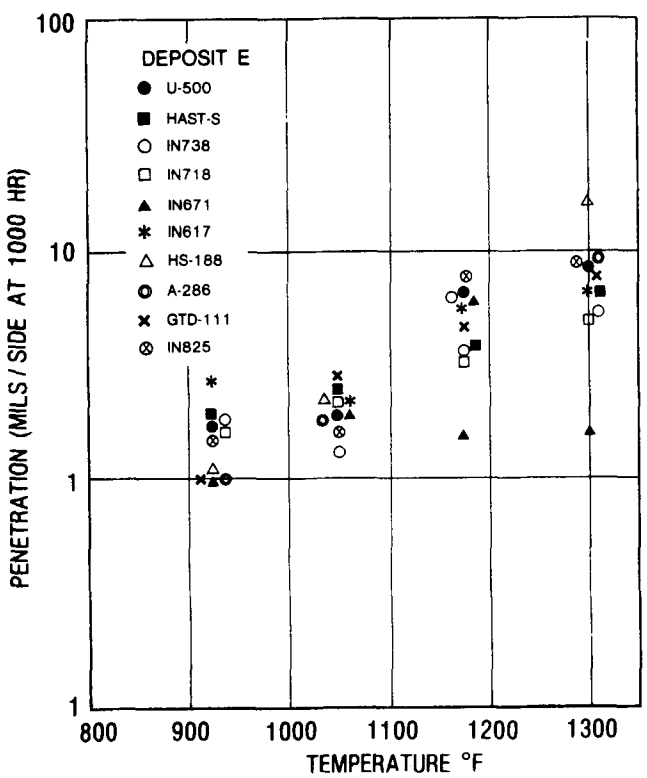

Fig. 7—Penetration with deposit E at 925 to 1300 °F.

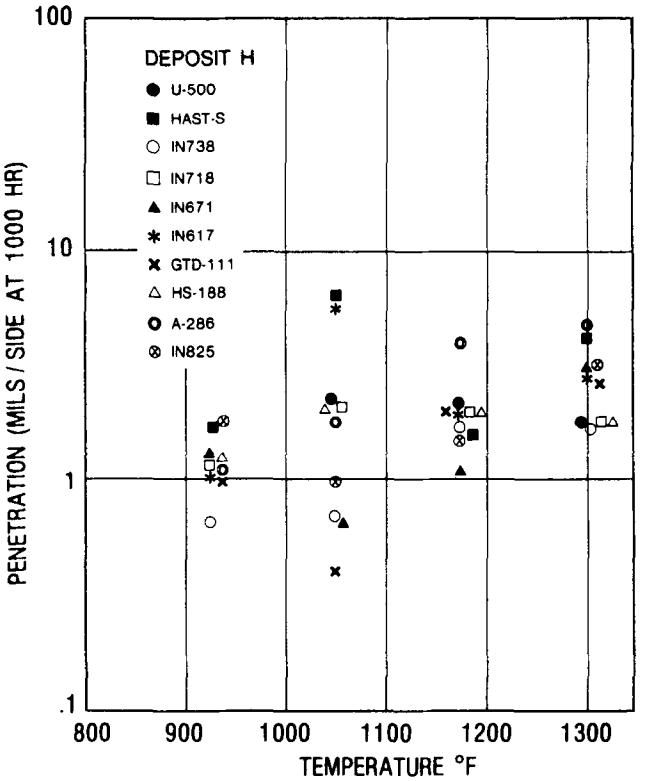

Fig. 8—Penetration with deposit H at 925 to 1300 °F.

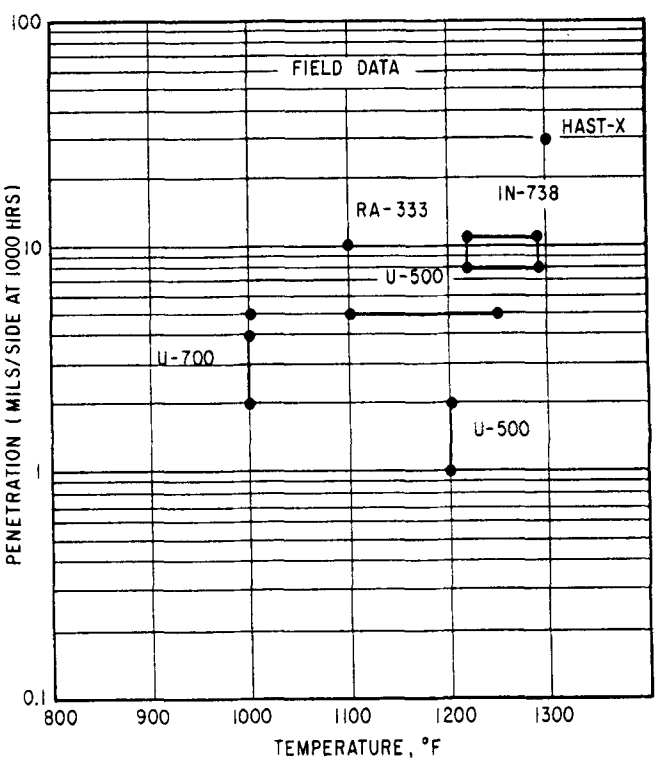

Fig. 9—Corrosion penetration derived from field observations. Extrapolated to 1000 hours by linear relationship; line connecting points indicates either a range of temperatures or penetrations.

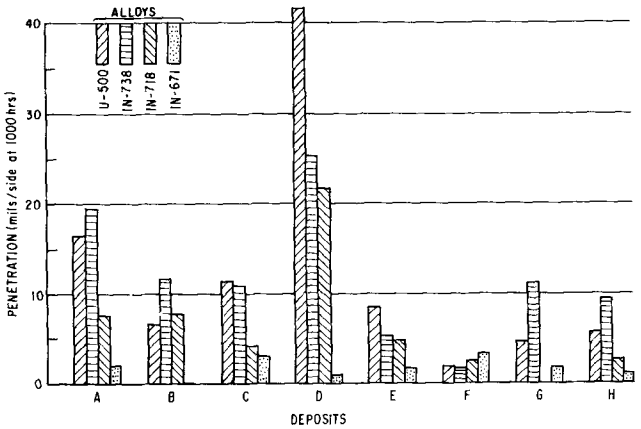

Fig. 10 — Comparison of performance of four alloys with various deposits at 1300 °F.

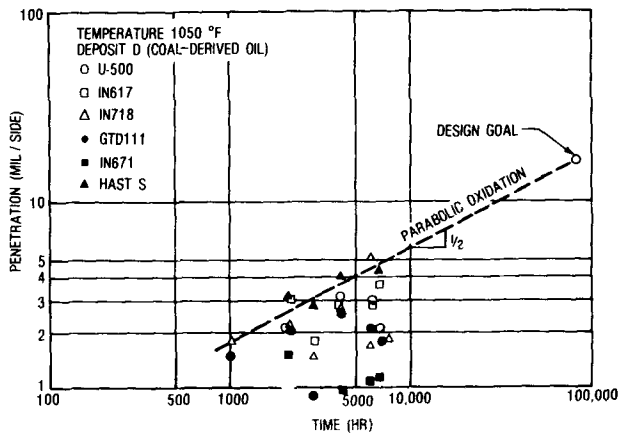

Fig. 11 — Time dependence of penetration with deposit D at 1050 °F.

500, IN-718, and IN-671) with different deposits. Clearly deposit D is the most aggressive and deposit H the least.

Long Term Exposure Test

In order to determine the time dependence of penetration so that extrapolation of test data could be compared with the design criteria of 15 mils (380μm) penetration in 83,000 hours, long term tests were carried out for a series of alloys with deposit D. The deposit D was chosen because it was most aggressive above 1100 °F (590 °C) and is representative of the ash from a coal-derived liquid. Therefore, it would provide both a realistic and a conservative estimate of long time performance at lower temperatures. Exposure tests were made at two temperatures, 925 °F (500 °C) and 1050 °F (570 °C), with a duration of time of up to 7000 hours. The values of penetration are listed in Table IV and the data are plotted in Figures 11 and 12 as logarithm of time (hours) versus logarithm of penetration (mils).

If corrosion follows a parabolic dependence on time, the depth of penetration ΔP is represented by $(\Delta P)^2 = K\ t$, where K is a constant and t is time. Arbitrarily adopting a $t^{1/2}$ dependence as representative of a rate which decreases with time, a dashed line with a slope of ½ has been extended from the design goal point of 15 mils (380μm) in 83,000 hours on Figures 11 and 12. It is noted that most of the data points fall below the dashed line, suggesting that several alloys might meet or exceed the design criterion, if deposit D at these temperatures and the chosen time dependency are representative of water-cooled turbine conditions. Each of the data points in Figures 11 and 12 represents a separate sample. At 1050 °F (570 °C) the most severely attacked alloy, Hast-S followed a projected parabolic rate, while the others fall, below the parabolic slope of ½. At 925 °F (500 °C), however, there is a considerable scatter of penetration and on some alloys less penetration was observed at longer exposures than at shorter exposures.

Table IV. Penetrations for Long-term Tests with Deposit D. (Mils per Side)

Temp (°F)	925 °F					1050 °F				
Time (hours)	1461	2132	4124	6020	7165	1000	2132	4030	6020	6716
Alloy										
U-500	1.0	2.1	2.8	3.1	1.9	—	2.1	3.15	3.1	3.1
IN-617	1.0	2.7	2.85	1.7	2.0	—	3.0	2.85	2.8	3.6
IN-718	1.9	1.7	1.8	0.9	1.7	1.85	2.2	2.7	1.7	1.8
GTD-111	1.0	2.3	2.2	1.5	1.3	1.5	2.0	2.6	2.1	1.8
IN-671	0.7	1.5	1.3	1.6	1.25	0.55	1.5	0.92	1.1	1.2
Hast-S	—	3.2	2.75	—	1.6	—	3.2	4.0	5.1	4.2

DISCUSSION

In order to determine the temperature dependence of corrosion penetration, the logarithmic penetration (mils/side at 1000 hours) was plotted against reciprocal Kelvin temperature in Figure 13. In each deposit the straight line band is divided into two sections at the critical temperature around 1050 °F (570 °C). Although the extent of corrosion in the low temperature region is extremely small and lacks

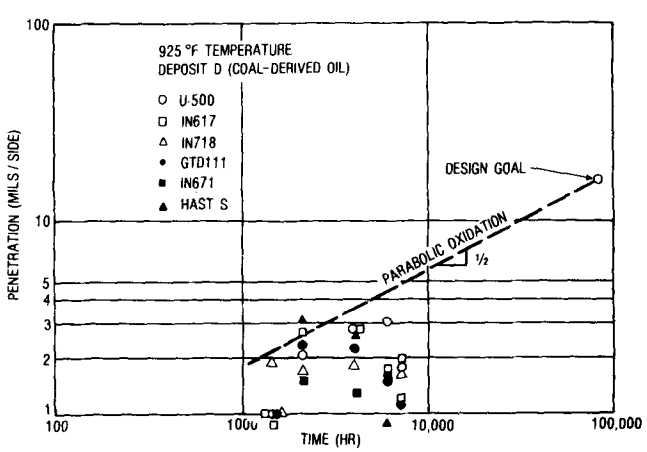

Fig. 12 — Time dependence of penetration with deposit D at 925 °F.

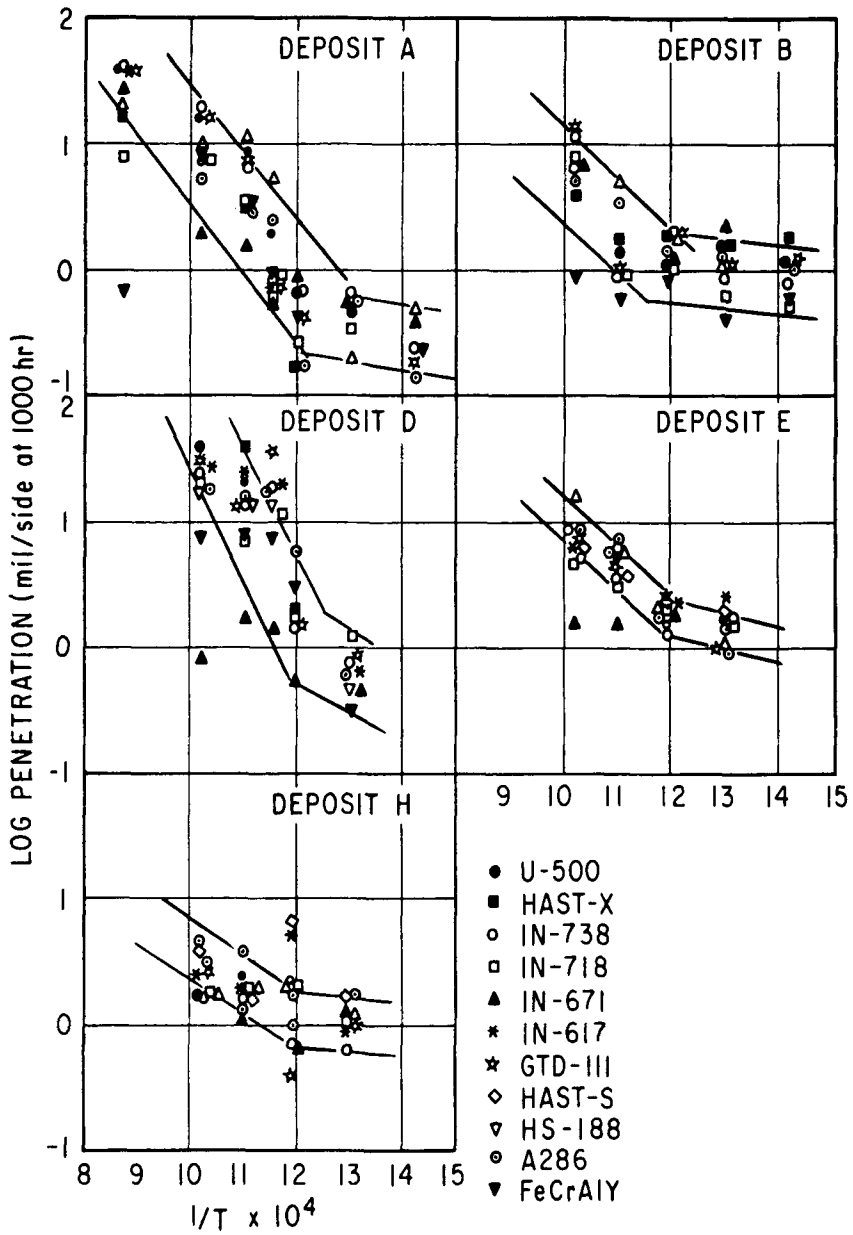

Fig. 13—Plot of logarithmic penetration against reciprocal Kelvin temperature.

sufficient accuracy to permit theoretical treatment of the corrosion behavior, it is obvious that the slope of the curve is much smaller than that in the high temperature region. The slopes of curves in the high temperature region correspond to activation energies between 13 to 36 Kcal/mole, but the corrosion processes are too complex to be represented in terms of a single rate-determining step. However, it is noted that the slope is very roughly proportional to the aggressiveness of the deposit, such as that demonstrated by the height of the bar-graphs in Figure 10. Deposit D gives the highest slope while deposit H the lowest.

Deposit E is the lowest melting point mixture of Na, K, and Mg sulfates according to a known phase diagram.[2] All of these metals are expected to be present in the combustion products of coal-derived fuels. Na and K sulfates cause hot corrosion at high temperatures around 1600 to 1700 °F (870 to 930 °C). Mg sulfate lowers the melting point of the Na, K, Mg sulfate mixture, thus, indirectly contributing to the corrosivity of the ternary deposit at lower temperatures. Significant attack was observed at 1175 °F (640 °C) and 1300 °F (700 °C) without producing internal oxides or sulfide precipitates characteristic of hot corrosion at high temperature. Typical photomicrographs of cross-sections after exposure are shown in Figures 14 and 15. Comparisons among several alloys with the data for deposit D at 1175 °F (640 °C) and 1300 °F (700 °C) revealed significantly increased attack compared to deposit E. This finding is consistent with the current concept that lead, which was present in deposit D, should be regarded as an aggressive component; whereas Mg appears to be innocuous.

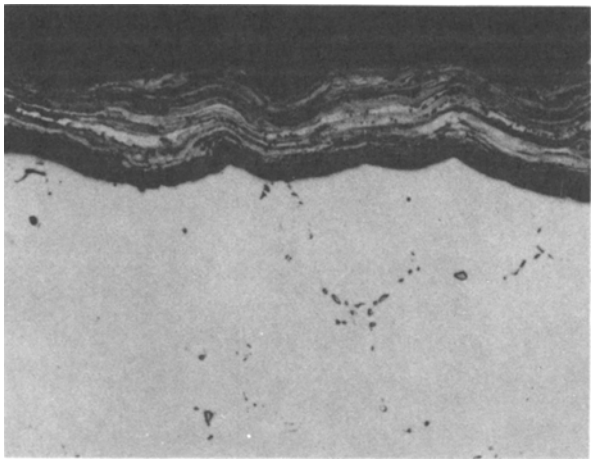

Fig. 14 — Cross-section of U-500 after 1074 hours at 1300 °F with deposit E, 250 times, as polished.

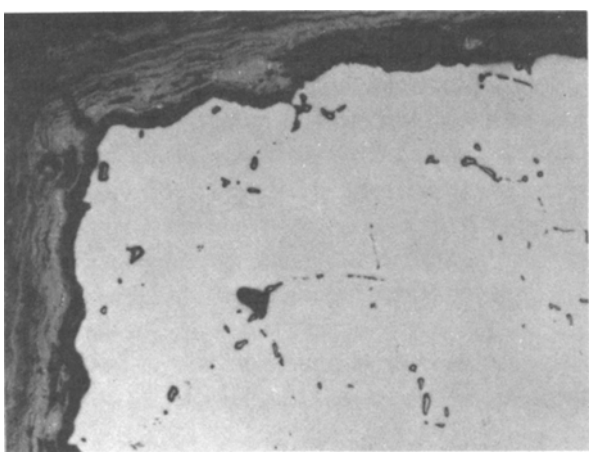

Fig. 15 — Cross-section of IN-738 after 1074 hours at 1175 °F with deposit E, 250 times, as polished.

Because of the apparent correspondence between the onset of rapid attack and the occurrence of a liquid phase in the deposit, differential thermal analysis (DTA) was carried out on deposits D and E to determine their melting temperatures. For deposit E a melting range of 1112 to 1202 °F (600 to 650 °C) was found (cooling, 10 deg/min), and correspondingly samples tested below 1100 °F (590 °C) were attacked very little; whereas significant attack occurred above that temperature. On the other hand, DTA for deposit D yielded a melting point of 1535 to 1544 °F (835 to 840 °C), but substantial attack occurred with this deposit at temperatures down to 1112 °F (600 °C). It was clear the deposit had melted well below the determined melting point. This apparent discrepancy is explained by noting that the deposit may interact with nickel or cobalt sulfates which form by reaction of the oxide scale with SO_3, to yield low melting liquid sulfate mixtures. It has been confirmed in independent studies that a liquid phase forms at 1380 °F (750 °C) from a deposit of pure Na_2SO_4 (M. P. 1623 °F (884 °C)) by reaction with $CoSO_4$ on a Ni-base superalloy containing Co.

The deposit which is expected from H-Coal Boiler Grade fuel consists of Na, K, Mg, Ca, and Pb sulfate. The composition is listed in Table I under F. Because of the complexity of the simulated deposit, a substantial effort has been made to ensure the desired composition in the coatings. For best results, two separate spraying solutions were mixed immediately before application. However, chemical analyses revealed that the spray solutions actually used had been incorrectly prepared to include 10 times the recommended lead content. Therefore, the composition designated as deposit H was actually used throughout the testing. Considering the level of Pb, the amount of attack at 1175 and 1300 °F (640 and 700 °C) is surprisingly small when compared with that found with deposit D at these temperatures. One possible explanation for the low rate of attack is that Ca inhibited Pb by the formation of calcium plumbate, Ca_2PbO_4. This species was identified by the X-ray diffraction analysis, along with some PbO and MgO.

The attack with deposit I, pure Na_2SO_4, is understandable due to the formation of a $CoSO_4-Na_2SO_4$ or $NiSO_4-Na_2SO_4$ liquid phase. A significantly reduced attack was observed in deposit J, which was simply deposit D with Ca added in an amount equal to Pb. These data support the contention that Ca, as well as Mg, is an effective inhibitor to the effect of Pb. According to Zetlmeisl,[3] corrosion of U-500 in the molten $PbO-V_2O_5$ system is effectively inhibited by the addition of magnesium at a composition of $Mg/(Pb + V) = 3$ to 4, up to the temperature of 1560 °F (850 °C) in crucible tests, but not under a sulfur containing atmosphere. Solid Mg-Pb-O and Mg-V-O compounds may form under such conditions. However, judging from the significant penetrations found with deposit E, magnesium is not an effective inhibitor for $(Na/K)_2SO_4$-induced attack, because solid compound formation is not expected. The role of $MgSO_4$ in deposit E apparently was to form a low melting liquid phase.

Oxidation characteristics of the superalloys are generally divided into two distinct groups with respect to the morphology, structure, and growth kinetics of the oxide scale. These two groups are distinguished as the Cr_2O_3-former and the Al_2O_3-former, and distinctive nature is predicted to a certain extent from the Ni-Cr-Al ternary oxide scale diagram. Generally the oxidation rate of the Cr_2O_3-formers is higher than that of the Al_2O_3-formers, and a parabolic rate law is obeyed when a dense Cr_2O_3 layer acts as a diffusion barrier.

The chromium content of all the tested alloys falls in a fairly narrow range between 14 and 25 wt. pct, except for IN-671 which has 50 pct chromium, and they may be regarded as Cr_2O_3-formers. Cr is considered the most important element beneficial to hot corrosion resistance,

however, the correlation of penetration with the composition is generally not simple in complex alloys. No other single element, such as Al or Ti, was found distinctively beneficial to all deposits. The chromium dependence of hot corrosion attack in each deposit is illustrated at 1300 °F (700 °C) in Figure 16, where the values for penetration in mils per side at 1000 hours are plotted against the Cr content of the alloys.

Despite some scattering, an approximate linear relationship appears to hold up to 50 pct Cr, which represents IN-671. Some discrepancies are seen, such as IN-671, which contains highest chromium of the group, shows the best overall performance, but poor resistance in deposit A at low temperatures; worst at 1050 °F (570 °C) in deposit A and at 925 °F (500 °C) in deposit B. Heavier corrosion is seen when the deposit contains lead as shown for IN-671 in deposits A, C and H. This is probably due to depletion of chromium from the alloy to form $PbCrO_4$.

The depth of penetration for rating alloys for service is the most direct index in corrosion measurements. It is based on the assumption that a loss in metal thickness corresponds to the amount of metal converted to oxides. However, there are some uncertainties associated with the measurements such as, accuracy in measurements, incomplete mass balance at the metal-oxide interface or volume change due to metallurgical transformation.

When the penetration depth is very small, the measurement is generally difficult and limited in accuracy since it can be performed only once in a destructive way and it is impossible to make the before and after measurement at the same location of the specimen. The accuracy of the measurement depends on the precision of the initial and final

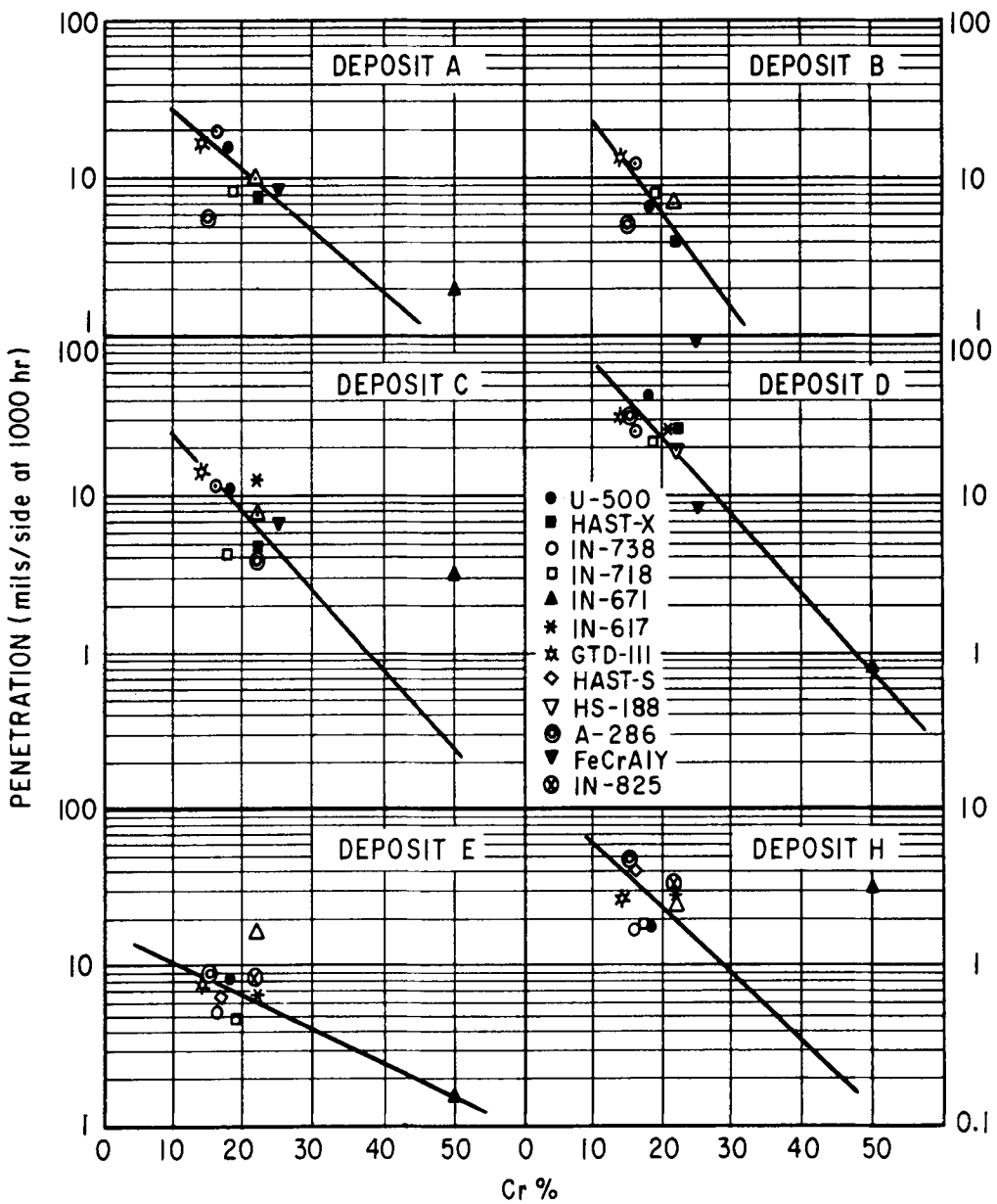

Fig. 16—Penetration and chromium content of alloys at 1300 °F.

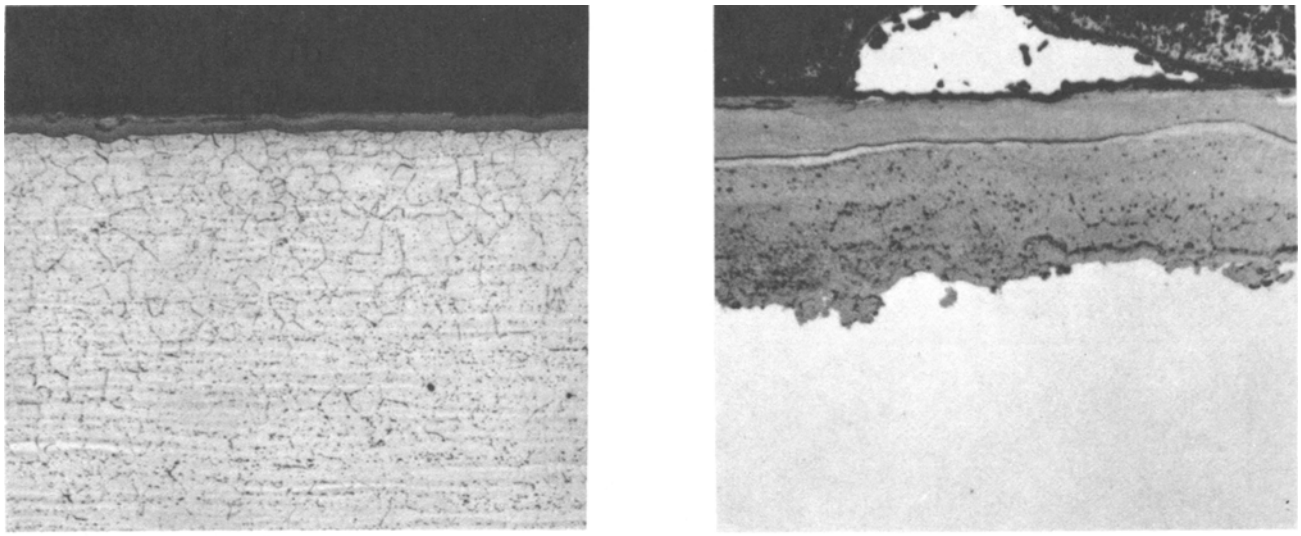

(a) (b)

Fig. 17—Cross-section of Hast-S exposed in deposit D after (*a*) 4124 hours at 925 °F (200 times, etched), and (*b*) 6716 hours at 1050 °F (250 times, as polished).

thickness measurements. Metallographic polishing tended to round the edges of the sample, leading to an underestimation of the final thickness and hence to an overestimation of the penetration. Perhaps a fair estimate of the overall error from the measurement technique would be +0.8 to +0.2 mils (+20 to +5μm). When the measurement is as small as 1 mil (25μm), as for the 7000 hour data at 925 °F (500 °C), the data should be viewed only as representing very low penetration rates.

Metallographic examination of the alloys tested for 4000 and 7000 hours showed little evidence of attack such as an irregular surface, an oxide scale, or internal precipitates. Figures 17 and 18 show typical examples for two temperatures on Hast-S and U-500. Etching did not reveal the presence of any appreciable internal corrosion or alloy depletion. Electron-microprobe analysis revealed that the oxide consisted of double layer structure, inner Cr-rich and outer Ni-rich, but no appreciable Cr depleted zone was detected.

Finally, the important parameters affecting accelerated attack at low temperatures are summarized as:

(a) the temperature for the appearance of a liquid phase on a particular alloy,
(b) the role of various contaminants in the corrosion process, and
(c) the role of contaminants in the atmosphere.

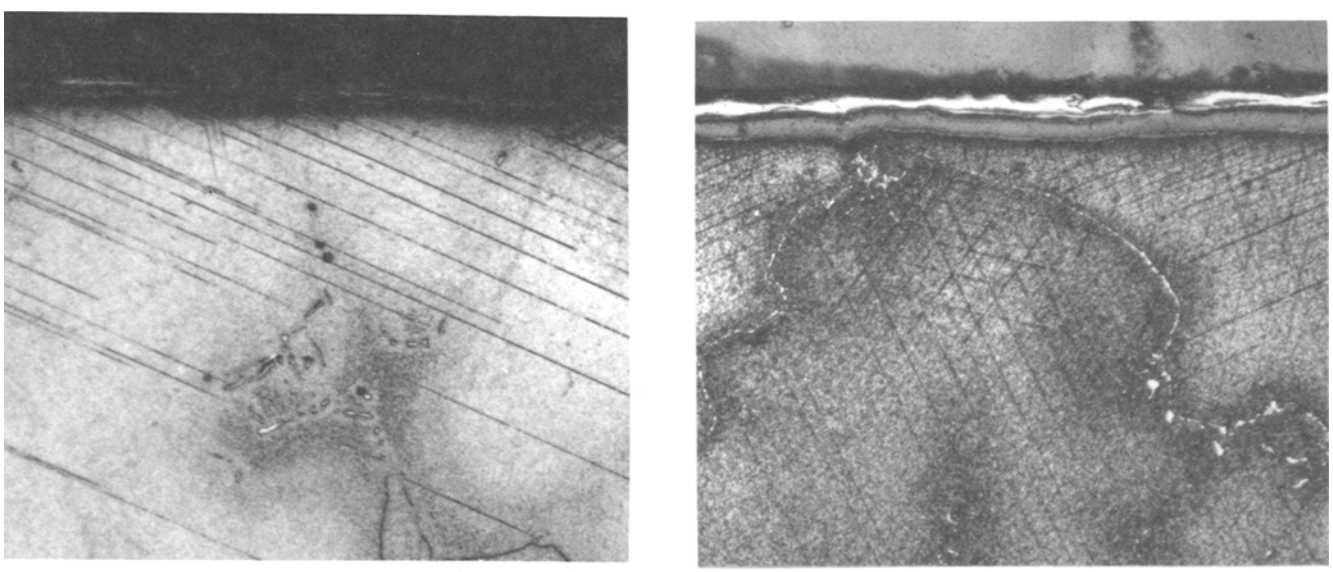

(a) (b)

Fig. 18—Cross-section of U-500 exposed in deposit D after (*a*) 6020 hours at 925 °F, and (*b*) 6020 hours at 1050 °F (200 times, etched).

The bulk composition of a deposit is much less important than is the composition of the liquid phase formed from it, since there is little evidence of aggressive attack from a completely dry deposit. The appearance of a liquid phase obviously depends on temperature, but for a given temperature it also depends on the substrate and on the composition of the atmosphere. The role of various components in the liquid phase may be categorized as either "active" or "passive". Sodium and potassium as sulfates are certainly active or aggressive components as are vanadium and lead. When Na_2SO_4 is present in predominance, V and K also tend to lower the melting point. Other components, such as $MgSO_4$, $CaSO_4$ or $CoSO_4$, appear to be passive in the sense that they themselves do not enhance the corrosion rate. However, they may lower the melting point sufficiently that accelerated attack will occur at a low temperature which otherwise would have been quite safe. As noted before, Ca (and Mg) may inhibit the effects of Pb in an alkali sulfate deposit; Mg is well known as an inhibitor of the effect of V. Components in the atmosphere may also play an important role. The formation of transition metal sulfates in the presence of SO_2 has been mentioned. In other independent studies the presence of trace amounts of Cl_2 or HCl was shown to lead to greatly accelerated attack at low temperatures with Na_2SO_4 deposits.

CONCLUSIONS

The composition of the condensate formed during the combustion of typical fuels in gas turbines was predicted by a computer program using available thermodynamic data. Hot corrosion tests were carried out in which candidate alloys coated with simulated deposit were exposed at temperatures ranging from 800 to 1300 °F (430 to 700 °C). The results showed that there is a critical temperature of 1050 °F (570 °C), above which the rate of corrosion becomes significantly high. Long term exposure tests were conducted at 1050 and 925 °F (570 and 500 °C). The test results showed that several alloys may meet or exceed the design requirements for the surface of a water-cooled turbine blade in the chosen deposit. IN-671 exhibited an overall-best performance against corrosion among the candidate alloys.

ACKNOWLEDGMENT

This work was supported by the Electric Power Research Institute under Contract RP234-3. The authors wish to thank H. S. Spacil, R. D. Lilliquis, and H. von E. Doering for their significant contributions to this work.

REFERENCES

1. S. Gordon and B. J. McBride: "Computer Program for Calculation of Complex Chemical Equilibrium Compositions", NASA SP-273, 1971.
2. E. M. Levin, *et al:* "Phase Diagram for Ceramists", Am. Ceram. Soc., Figs. 2914-5, 1969.
3. M. J. Zetlmeisl, *et al:* "High Temperature Corrosion in Gas Turbines and Steam Boilers by Fuel Impurities", Trans. ASME, *J. Eng. Power,* 74-WA/CD-4, 1974.